Electronic Supplementary Information (ESI)

Helix-constructed Polar Rare-earth Iodate Fluoride as Laser Nonlinear Optical Multifunctional Materials

Guang Peng,[ab] Yi Yang,[c] Tao Yan,*[ab] Dan Zhao,[d] Bingxuan Li,[ab] Ge Zhang,[ab] Zheshuai Lin[c] and Ning Ye*[ab]

[a] Key Laboratory of Optoelectronic Materials Chemistry and Physics, Fujian Institute of Research on the Structure of Matter, Chinese Academy of Sciences, Fuzhou, Fujian 350002, China
[b] Fujian Science & Technology Innovation Laboratory for Optoelectronic Information of China, Fuzhou, Fujian 350002, China
[c] Beijing Center for Crystal R&D, Key Lab of Functional Crystals and Laser Technology of Chinese Academy of Sciences, Technical Institute of Physics and Chemistry, Chinese Academy of Sciences, Beijing 100190, China
[d] College of Chemistry and Chemical Engineering, Henan Polytechnic University, Jiaozuo, Henan 454000, China

Table of Contents

Experimental Procedures
Table S1. Crystal data and structure refinement for YIF
Table S2. Atomic coordinates and equivalent isotropic displacement parameters for YIF
Table S3. Selected bond lengths and angles for YIF
Table S4. Anisotropic displacement parameters for YIF
Table.S5 Calculated linear and nonlinear optical properties at the wavelength of 1064 nm.
Table S6 Fluorescence properties of RE-doped YIF crystals.
Figure S1. Powder XRD patterns analysis of YIF (a) and RE:YIF (b)
Figure S2. The Energy dispersive X-ray spectroscope (EDS) analysis for YIF
Figure S3. Thermogravimetric analysis (TGA) of YIF
Figure S4. Powder XRD analysis for the residual of YIF after heating at 1100 ^{o}C
Figure S5. The UV-vis-NIR diffuse reflectance spectra of YIF
Figure S5. The IR spectra of YIF
Figure S7. The converted F(R)-versus-Energy plot of YIF
Figure S8. The calculated band gap of YIF
Figure S9. The partial and total density states (PDOS and DOS) of YIF

Experimental Procedures

Crystals Growth

Reagent

The Rare earth oxides (Y_2O_3, Pr_2O_3, Nd_2O_3, Dy_2O_3, Ho_2O_3, Er_2O_3, Tm_2O_3, and Yb_2O_3, 99.99%), HIO_3 (99.0%), HF(49%), and boron trifluoride dihydrate (65% BF_3) were purchased from Shanghai Titan Scientific. Co., Ltd. All these starting materials were used without further treatment.

Synthesis

The YIF crystals were synthesized by mild hydrothermal method. The reaction materials Y_2O_3 and HIO_3 in a molar ratio of 1 : 3~5 were mixed with a moderate amount of deionized water and HF or $BF_3{\cdot}2H_2O$ as fluorating agent, which were then sealed in an autoclave with a Teflon liner (23 mL) and heated at 240 ^oC for 5 days, followed by slow cooling to 25 ^oC at a rate of 5 $^oC{\cdot}h^{-1}$. After washed with deionized water and dried in the air, the colorless, transparent, and non-hygroscopic hexagonal YIF crystals were obtained in a yield of about 95 % according to Y. The active ions doped RE : YIF (RE = Pr, Nd, Dy, Ho, Er, Tm, and Yb) crystals were also synthesized by the same method with different molar concentrations (Pr (1, 2, 4 mol%), Nd (3, 6, 9 mol%), Dy (5, 9, 13 mol%), Ho (1.5, 5, 10 mol%), Er (1, 15, 50 mol%), Tm (5, 10, 15 mol%), and Yb (3, 6, 9 mol%)) of rare-earth oxides were added.

Physical Measurements

Single crystal X-ray diffraction data was collected on a Rigaku Mercury CCD diffractometer equipped with graphite-monochromatic Mo Kα radiation (λ = 0.71074 Å) at room temperature. The data was integrated by the CrystalClear program. The data intensities were corrected for Lorentz polarization, air absorption, and absorption attributable to the variation in the path length through the detector faceplate. Multiscan technique was applied for absorption corrections. The crystal structure of YIF was determined by the direct methods and refined by full-matrix least-squares fitting on F^2 using SHELXS crystallographic software package. All atoms were refined with anisotropic displacement parameters. The TWIN and BASF instructions were used. The structure was checked by PLATON, and no higher symmetry was found. The crystallographic data are tabulated in Table S1. Atomic coordinates and equivalent isotropic displacement parameters, selected bond lengths and angles, as well as anisotropic displacement parameters for YIF are listed seriatim in Table S2-S4 in the Supporting Information.

The X-ray diffraction (XRD) pattern of polycrystalline powder in the angular range of 2θ=5−85° was obtained on a Miniflex-600 powder X-ray diffractometer by using Cu Kα radiation (λ = 1.54059 Å) with a scan step width of 0.02° and a fixed counting time of 0.2 s per step at room temperature. The powder XRD patterns of rare-earth ions doped RE: YIF (RE = Pr (4 mol%), Nd (9 mol%), Dy (13 mol%), Ho (10 mol%), Er (50 mol%), Tm (15 mol%), and Yb (9 mol%)) crystals in the angular range of 2θ=20−60° were obtained.

The elemental composition analysis were performed on a field emission scanning electron microscope (FESEM, SU-8010) equipped with an energy dispersive X-ray spectroscopy (EDS). Several YIF crystals were carefully washed by deionized water and alcohol, and then mounted on an aluminum sample stage by carbon conductive tape. The accelerating voltage and emission current were set to 20 kV and 12 μA, respectively.

The thermogravimetric analysis (TGA) of YIF was conducted on a Netzsch STA449F3 simultaneous analyzer. The crystal sample and reference (Al_2O_3) were enclosed in Al_2O_3 crucibles and heated from 30 to 1300^{o}C at a rate of 10^{o}C/min under a constant flow of nitrogen gas.

The ultraviolet-visible-near-infrared (UV-Vis-NIR) diffuse reflectance spectra of YIF were measured on a PerkinElmer Lamda-950 UV/Vis/NIR spectrophotometer at room temperature in the range of 190-2500 nm with $BaSO_4$ as the standard of 100% reflectance. The reflectance were converted to absorbance by the Kubelka-Munk function: $F(R) = (1-R)^2/(2R) = K/S$, where R is the reflectance, K is the absorption, and S is the scattering.[1]

The Fourier transform infrared spectroscopy (FTIR) spectrum of YIF was recorded on a Bruker VERTEX 70 infrared spectrometer in the range from 400 to 4000 cm^{-1}.

Powder SHG signals were measured by the Kurtz-Perry method with a 1064 nm Q-switched Nd:YAG laser under the same voltage.[2] The YIF and KDP (used as a reference) were ground and sieved into the following particle size ranges: 25-45, 45-62, 62-75, 75-109, 109-150, and 150-212 μm. The samples were pressed between two rounded 1 mm thick sheet glasses with a 2 mm thick rubber ring interlayer containing an 8 mm diameter hole in the middle, and then tightly sheathed in an aluminous round box with an 8mm diameter hole in the middle. A cutoff filter was used to limit background flash-lamp light on the samples. An interference filter (530 ± 10 nm) was used to select the frequency-doubled light from the samples. The intensities of the SHG signals were measured using a photomultiplier tube attached to a RIGOL DS1052E 50 MHz oscilloscope.

The LDT values of YIF and $AgGaS_2$ (AGS) in the particle-size range of 150-212 μm were evaluated under the same laser source (1064 nm, 10 ns, 1 Hz). This measurement method using powder samples has been confirmed to be feasible for preliminary evaluation.[3]

The excitation and emission spectra were measured by a fluorescence spectrometer (FLS980, Edinburgh) at room temperature. The fluorescence decay curves were recorded by time correlated single photon counting (TCSPC) technique.

The Raman spectra in the range of 50~1500 cm^{-1} were obtained at room temperature on a LabRAM HR Evolution spectrometer (Horiba Jobin Yvon) under a laser excitation at 532 nm.

Computional methods

The first-principles calculation for YIF was performed by the CASTEP package based on the density functional theory (DFT).[4,5] The gradient generalized approximation (GGA) with the Perdew-Burke-Ernzerhof (PBE) functional was adopted to describe the exchange-correlation energy.[6] The optimized norm-conserving pseudopotentials[6] in the Kleinman-Bylander[7] form for all the elements (Y $4d^15s^2$, I $5s^25p^5$, O $2s^22p^4$, and F $2s^22p^5$) were used to model the effective interaction between atom cores and valence electrons. The high kinetic energy cutoff 850 eV and dense 4×4×2 Monkhorst-Pack *k*-point meshes in the Brillouin zones were chosen. Because of the discontinuity of exchange-correlation energy, the calculated band gaps by GGA-PBE were usually underestimated. Thus, a scissor operator[8] was adopted to shift all the conduction bands to match the calculated band gaps with the measured value for the optical properties calculations. Based on the scissor-corrected electron band structure, the imaginary part of the dielectric function was calculated, and the real part was obtained by the Kramers-Kronig transform,[9] and then the refractive index was determined. The SHG coefficients d_{ij} were obtained by the formula originally proposed by Rashkeev *et al*[10] and developed by Lin *et al*.[8] The the SHG-weighted charge density analysis tool and the real space atomic cutting technique were adopted to evaluate the SHG/birefringence-contribution of IO_3 groups and YO_6F_2 polyhedra.[11-13]

Results and Discussion

Table S1. Crystal Data and Structure Refinement for YIF

Formula	$Y(IO_3)_2F$
Formula mass (amu)	457.71
Temperature (K)	293(2)
λ(Å)	0.71073
Crystal system	Hexagonal
Space group	P6(5)
a (Å)	6.8455(9)
c (Å)	21.807(5)
V (Å^3)	885.0(3)
Z	6
ρ(calcd) (g/cm^3)	5.153
μ (mm^{-1})	20.344
F(000)	1212
ϑ (deg)	3.437-27.463
Index range	$-7 \le h \le 8$, $-8 \le k \le 8$, $-28 \le l \le 27$
R_{int}	0.0939
Completeness to ϑ = 25.242	100.0%
GOF on F^2	1.108
R_1/wR_2 ($I>2\sigma(I)$)[a]	R_1 = 0.0503, wR_2 = 0.1078
R_1/wR_2 (all data)[a]	R_1 = 0.0515, wR_2 = 0.1084
Extinction coefficient	0.00050(17)

Table S2. Atomic coordinates (×10^4) and equivalent isotropic displacement parameters (Å^2×10^3) for YIF. U(eq) is defined as one third of the trace of the orthogonalized U_{ij} tensor.

Atom	x	y	z	U(eq)
Y(1)	-3297(6)	-3255(4)	1237(2)	12(1)
I(1)	3404(3)	-299(3)	1468(1)	12(1)
I(2)	-320(4)	3086(3)	1020(1)	15(1)
O(1)	220(40)	4210(30)	247(10)	20(5)
O(2)	-1960(40)	4160(40)	1338(10)	18(5)
O(3)	-2610(40)	290(30)	781(12)	35(6)
O(4)	-6880(30)	-2990(30)	1272(9)	10(4)
O(5)	3690(30)	-290(30)	2275(10)	17(4)
O(6)	550(40)	-980(40)	1429(13)	31(6)
F(1)	-2940(30)	-950(30)	1998(10)	33(5)

Table S3. Selected bond lengths (Å) and angles (degrees) for YIF

Y(1)-F(1)#1	2.14(2)	F(1)#1-Y(1)-O(5)#4	70.5(7)
Y(1)-F(1)	2.22(2)	F(1)-Y(1)-O(5)#4	143.6(7)
Y(1)-O(1)#2	2.33(2)	O(1)#2-Y(1)-O(5)#4	74.0(7)
Y(1)-O(6)	2.33(3)	O(6)-Y(1)-O(5)#4	143.6(8)
Y(1)-O(2)#3	2.37(2)	O(2)#3-Y(1)-O(5)#4	79.9(7)
Y(1)-O(5)#4	2.41(2)	F(1)#1-Y(1)-O(3)	70.1(8)
Y(1)-O(3)	2.44(2)	F(1)-Y(1)-O(3)	72.6(8)
Y(1)-O(4)	2.55(2)	O(1)#2-Y(1)-O(3)	139.6(8)
I(1)-O(6)	1.77(2)	O(6)-Y(1)-O(3)	79.5(9)
I(1)-O(5)	1.77(2)	O(2)#3-Y(1)-O(3)	145.5(8)
I(1)-O(4)#5	1.804(18)	O(5)#4-Y(1)-O(3)	108.2(8)
I(2)-O(2)	1.77(2)	F(1)#1-Y(1)-O(4)	113.1(7)
I(2)-O(1)	1.81(2)	F(1)-Y(1)-O(4)	72.3(6)
I(2)-O(3)	1.84(2)	O(1)#2-Y(1)-O(4)	72.3(7)
F(1)#1-Y(1)-F(1)	136.8(7)	O(6)-Y(1)-O(4)	138.8(7)
F(1)#1-Y(1)-O(1)#2	140.3(7)	O(2)#3-Y(1)-O(4)	142.5(8)
F(1)-Y(1)-O(1)#2	82.9(7)	O(5)#4-Y(1)-O(4)	74.1(6)
F(1)#1-Y(1)-O(6)	79.6(9)	O(3)-Y(1)-O(4)	69.9(7)
F(1)-Y(1)-O(6)	72.7(8)	O(6)-I(1)-O(5)	98.9(11)
O(1)#2-Y(1)-O(6)	123.5(9)	O(6)-I(1)-O(4)#5	100.3(10)
F(1)#1-Y(1)-O(2)#3	82.1(7)	O(5)-I(1)-O(4)#5	101.1(9)
F(1)-Y(1)-O(2)#3	120.8(8)	O(2)-I(2)-O(1)	102.9(10)
O(1)#2-Y(1)-O(2)#3	74.8(8)	O(2)-I(2)-O(3)	99.0(11)
O(6)-Y(1)-O(2)#3	75.7(9)	O(1)-I(2)-O(3)	93.7(11)

Symmetry transformations used to generate equivalent atoms:
#1 x-y,x,z-1/6; #2 y-1,-x+y-1,z+1/6; #3 x,y-1,z; #4 x-y-1,x-1,z-1/6; #5 x+1,y,z; #6 x-y,x+1,z-1/6; #7 x,y+1,z; #8 x-1,y,z; #9 y+1,-x+y,z+1/6; #10 y,-x+y,z+1/6

Table S4. Anisotropic displacement parameters ($Å^2 \times 10^3$) for YIF

The anisotropic displacement factor exponent takes the form: $-2\pi^2$ [$h^2 a^{*2}$ U11 + ... + 2hka* b*U12]

	U11	U22	U33	U23	U13	U12
Y(1)	10(1)	14(1)	9(1)	1(2)	4(1)	5(1)
I(1)	9(1)	15(1)	12(1)	-1(1)	0(1)	6(1)
I(2)	15(1)	19(1)	16(1)	2(1)	1(1)	12(1)
O(1)	22(6)	17(6)	13(7)	2(5)	1(5)	5(5)
O(2)	21(7)	17(6)	17(7)	1(5)	0(5)	11(5)
O(3)	32(12)	15(11)	50(18)	3(11)	-10(12)	7(10)
O(4)	10(6)	7(6)	9(6)	0(5)	2(5)	2(5)
O(5)	20(6)	13(6)	18(7)	0(5)	1(5)	8(5)
O(6)	28(7)	33(7)	41(8)	-1(5)	0(5)	22(5)
F(1)	16(9)	34(11)	20(12)	-13(9)	8(8)	-8(8)

Table.S5 Calculated linear and nonlinear optical properties at the wavelength of 1064 nm.

	d_{31}	d_{33}	n_x	n_y	n_z	Δn
$Y(IO)_2F$	**-0.64**	2.04	2.038	2.038	1.997	0.041
IO_3	**-0.83**	2.78	1.916	1.916	1.890	0.026
YO_6F_2	**0.07**	-0.18	1.402	1.402	1.392	0.010

Table S6 Fluorescence properties of RE-doped YIF crystals.

Sample		Conc. (mol)	Absorption		Emission		lifetime	Ref.
			Peak (nm)	FWHM (nm)	Peak (nm)	FWHM (nm)		
Dy	YIF	5.0%	452	6.0	576	10.2	285 µs	this
	YAG	3.0%	447	1.0	583	0.2	376 µs	14
	NGM	3.0%	454	7.0	574	9.6	152 µs	15
Pr	YIF	2.0%	448	16.0	602	14.2	35.4 µs	this work
	YLF	0.65%	444	1.8	607	1.5	35.7 µs	16
	YAP	0.6%	448	3.9	622	1.6	13.8 µs	17
Nd	YIF	3.0%	804	16	1057/1070	6.5/8.0	181 µs	this work
	YAB	4.0%	807	2	1062	3.2	60 µs	18
	YCOB	2.0%	812	2	1060	2.6	102 µs	19
	GdCOB	1.0%	811	1	1060	2.4	98 µs	20
Yb	YIF	3.0%	972	20	1054	20	0.75 ms	this work
	YAB	5.6%	976	22	1040	20	0.68 ms	21
	YCOB	20%	976	3	1032	44	2.28 ms	22
	GdCOB	15%	976	3	1030	90	2.44 ms	23
Er	YIF	1.0%	974	26	1546	58.0	4.0 ms	this work
	YAG	1.0%	N/A	N/A	1617/1645	N/A	7.7 ms	24
	YAB	1.5%	976	17	1550	N/A	0.3 ms	25
Tm	YIF	5.0%	1688	24	1815	145	0.90 ms	this work
	YAG	1.0%	N/A	N/A	2011	25	10.5 ms	26
	YLF	0.5%	N/A	N/A	1902	40	15.6 ms	26
	KLuW	5.0%	N/A	N/A	1841	90	0.9 ms	27
Ho	YIF	1.5%	1950	12	2040	140	3.1 ms	this work
	YAG	1.0%	N/A	N/A	2098	40	7.8 ms	26
	YLF	0.5%	N/A	N/A	2050	20	16.1 ms	26
Er	YIF	50%	978	33.5	2650/2795	70/80	0.08 ms	this work
	YAG	33%	N/A	N/A	2940	N/A	0.09 ms	28
	GGG	30%	N/A	N/A	2700	N/A	0.90 ms	29

N/A = not reported or not available

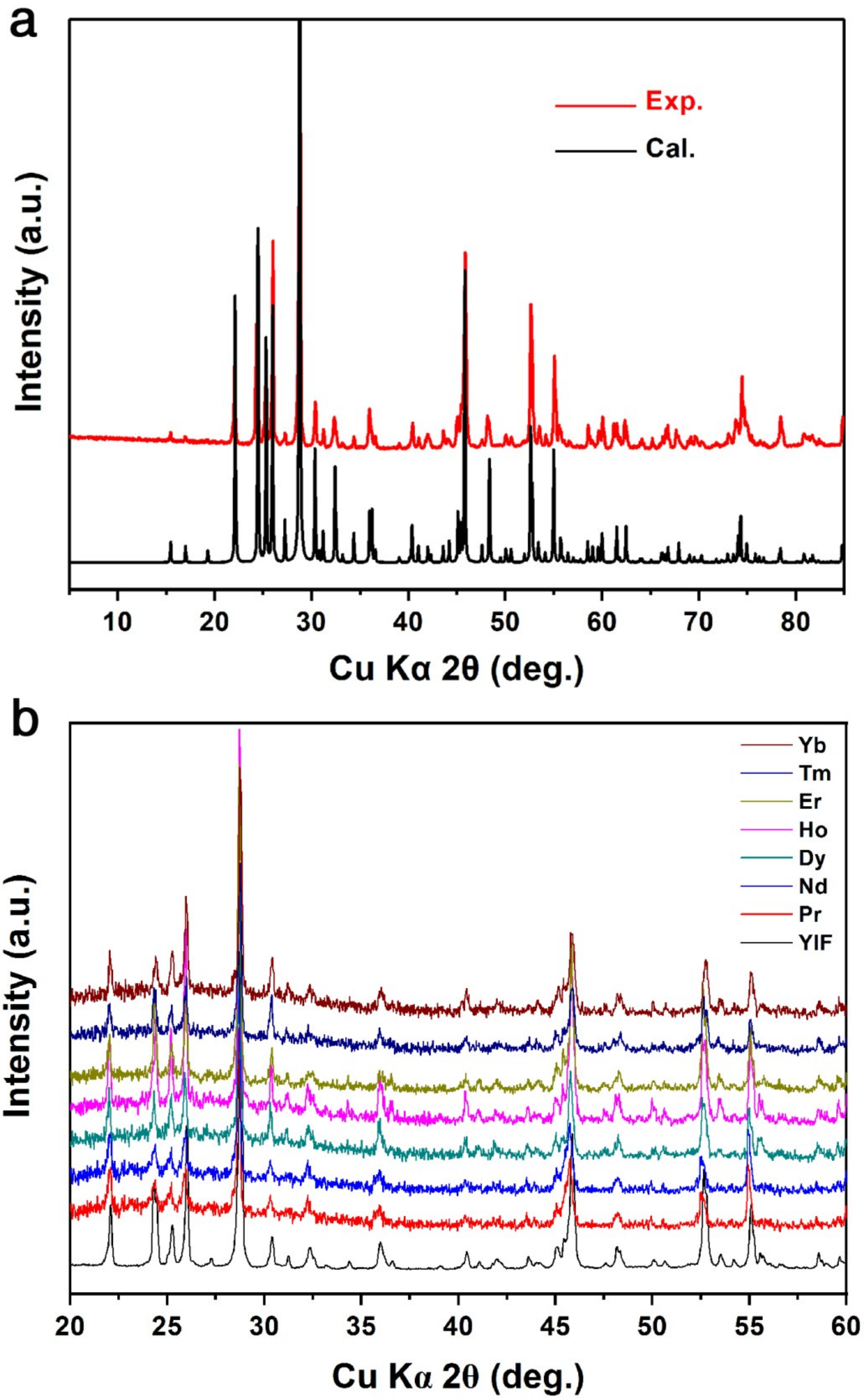

Figure S1. Powder XRD patterns analysis of YIF (a) and RE:YIF (b)

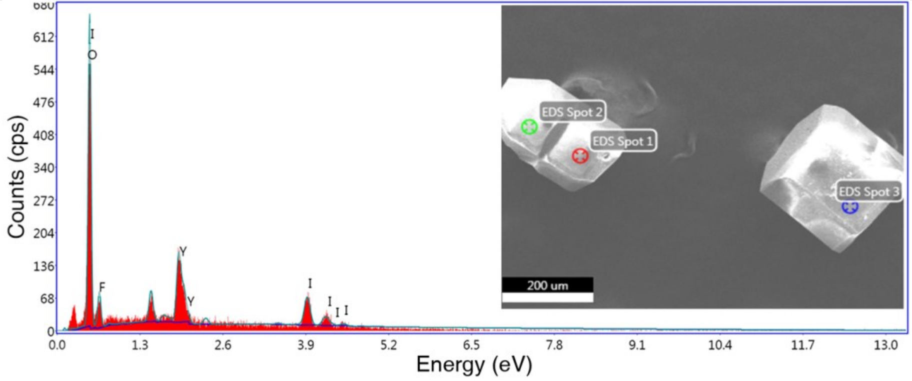

Figure S2. The Energy dispersive X-ray spectroscopy (EDS) analysis for YIF

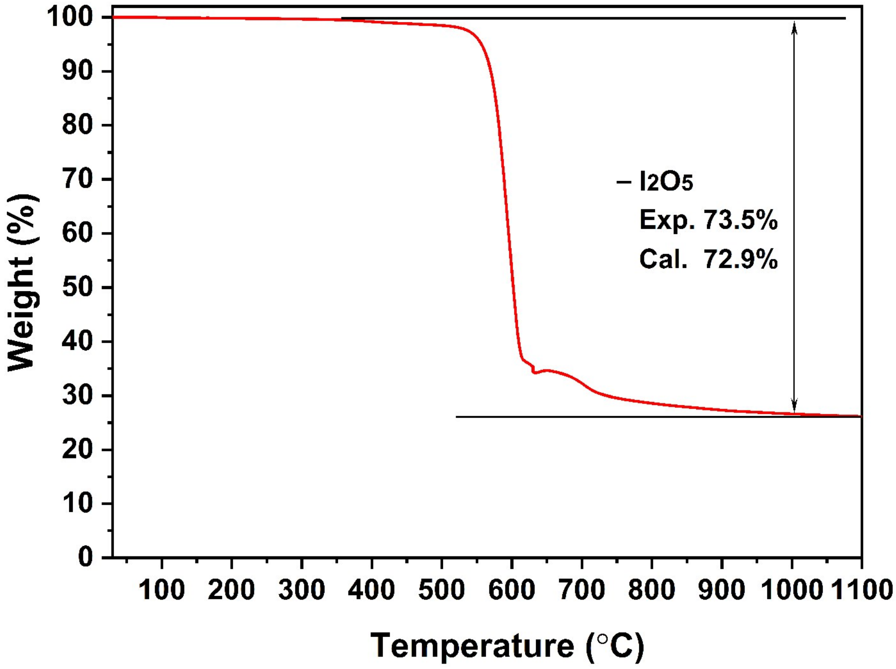

Figure S3. Thermogravimetric analysis (TGA) of YIF

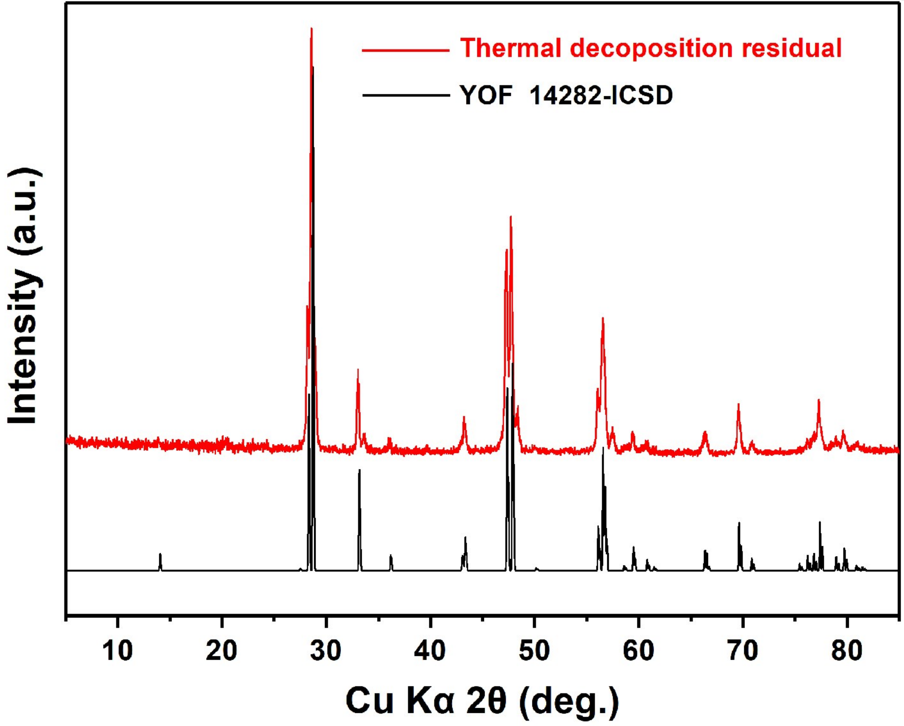

Figure S4. Powder XRD analysis for the residual of YIF after heating at 1100 ^{o}C

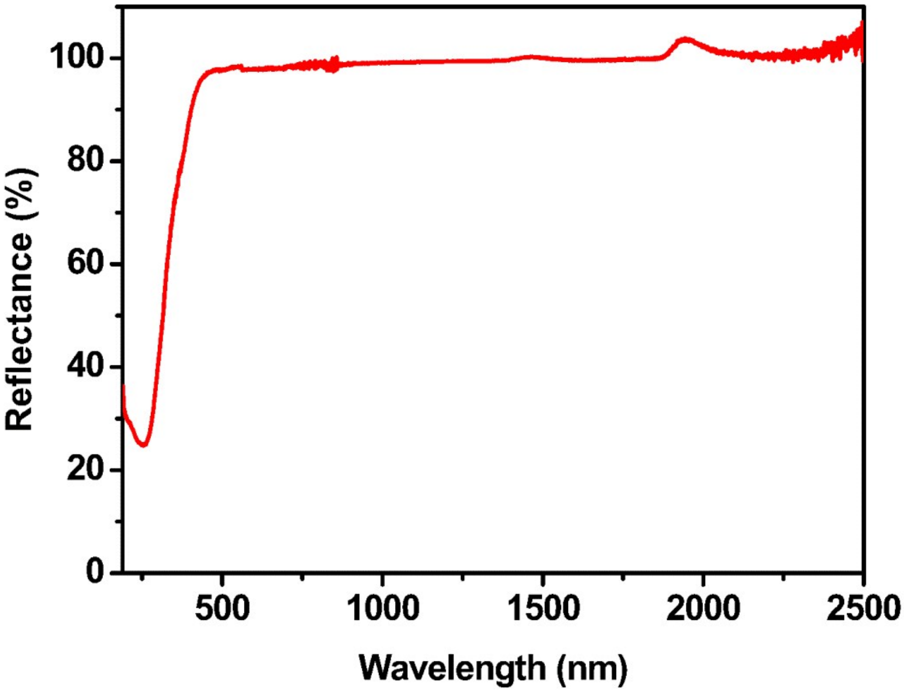

Figure S5. The UV-vis-NIR diffuse reflectance spectra of YIF

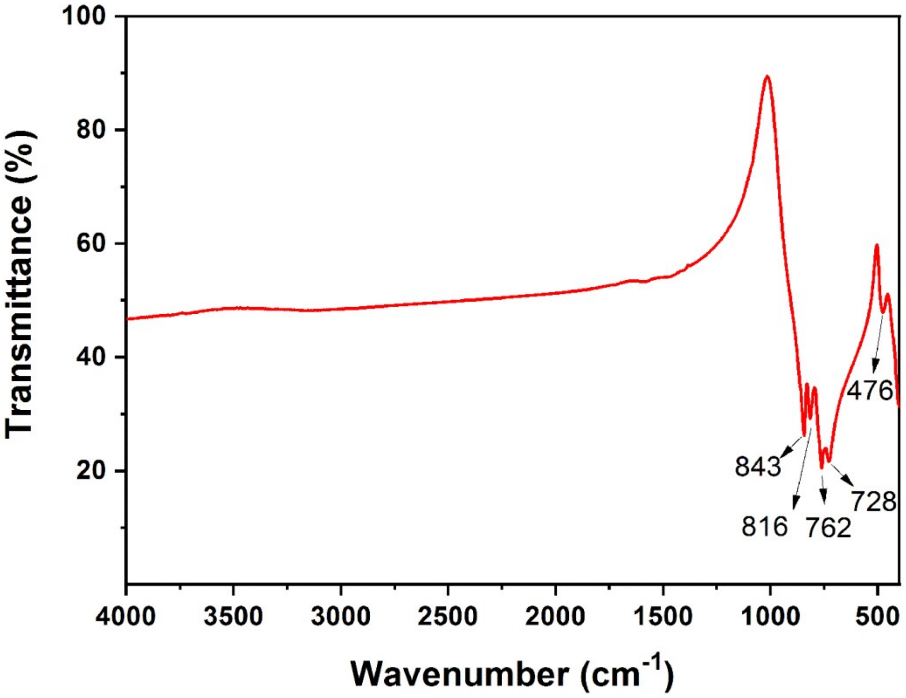

Figure S6. The IR spectra of YIF. The absorption bands at 843-728 cm^{-1} are mainly attributed to the stretching vibrations of IO_3 groups. Other bands at 476 and ~400 cm^{-1} can be assigned to Y−O/F vibrations.

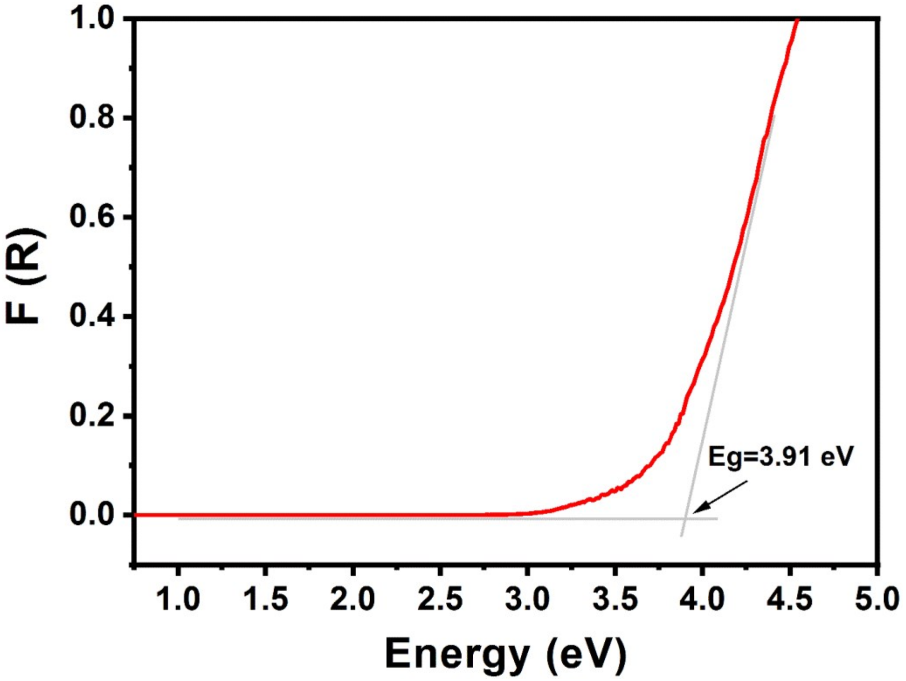

Figure S7. The converted F(R)-versus-Energy plot of YIF

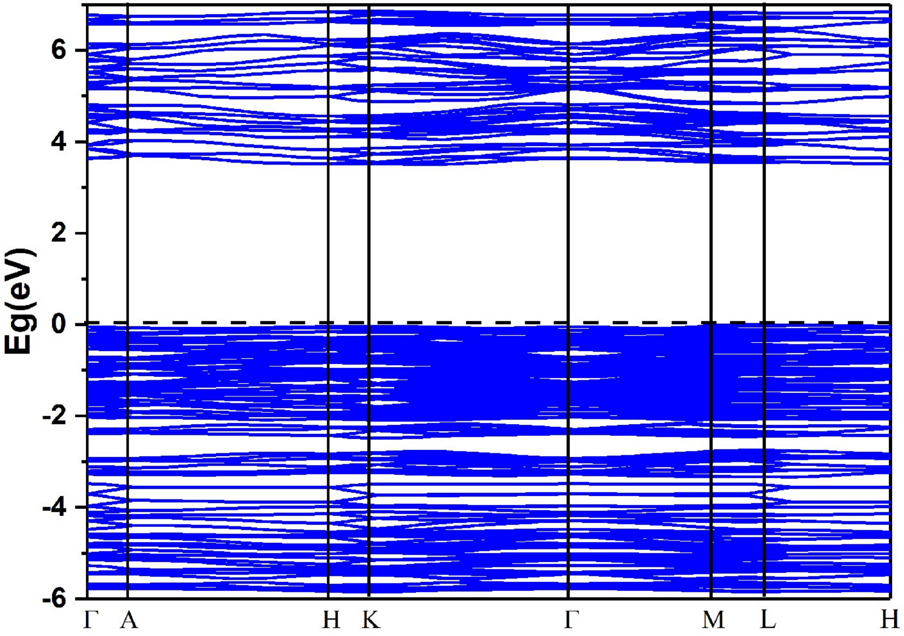

Figure S8. The calculated band gap of YIF

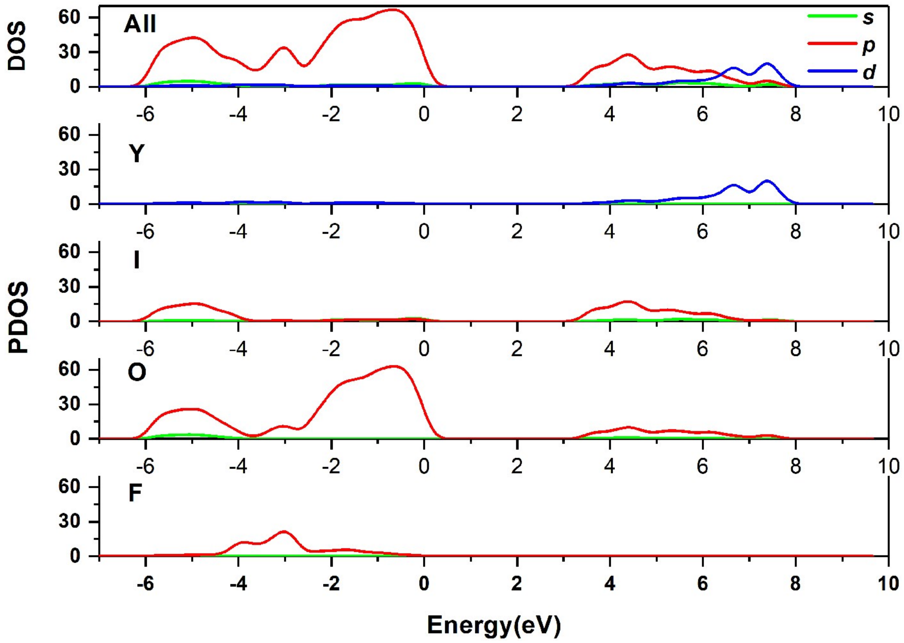

Figure S9. The partial and total densities states (PDOS and DOS) of YIF.

References

1. (a) P. Kubelka, F. Z. Munk, *Tech. Phys.* **1931**, 12, 593-601; (b) J. Tauc, *Mater. Res. Bull.* **1970**, 5, 721-729.
2. S. K. Kurtz, T. T. Perry, *J. Appl. Phys.* **1968**, 39, 3798-3813.
3. (a) J. A. Brant, D. J. Clark, Y. S. Kim, J. I. Jang, A. Weiland, J. A. Aitken, *Inorg. Chem.* **2015**, 54, 2809-2819; (b) D. Phanon, I. Gautier-Luneau, *Angew. Chem., Int. Ed.* **2007**, 46, 8488-8491; (c) M. Zhang, B. Li, B. Liu, Y. Fan, X. Li, H. Zeng, G. Guo, *Dalton Trans*. **2013**, 42, 14223-14229; (d) M. Zhang, X. Jiang, L. Zhou, G. Guo, *J. Mater. Chem. C* **2013**, 1, 4754-4760.
4. S. J. Clark, M. D. Segall, C. J. Pickard, P. J. Hasnip, M. J. Probert, K. Refson, M. C. Payne, *Z. Kristallogr.* **2005**, 220, 567-570.
5. M. C. Payne, M. P. Teter, D. C. Allan, T. A. Arias, J. D. Joannopoulos, *Rev. Mod. Phys.* **1992**, 64, 1045-1097.
6. A. M. Rappe, K. M. Rabe, E. Kaxiras, J. D. Joannopoulos, *Phys. Rev. B* **1990,** *41*, 1227-1230.
7. L. Kleinman, D. M. Bylander, *Phys. Rev. Lett.* **1982,** *48*, 1425-1428.
8. R. W. Godby, M. Schluter, L. J. Sham, *Phys. Rev. B* **1988,** *37*, 10159-10175.
9. E. D. Palik, *Handbook of Optical Constants of Solids*. Academic Press: New York, **1985**.
10. S. N. Rashkeev, W. R. L. Lambrecht, B. Segall, *Phys. Rev. B* **1998**, 57,3905.
11. J. Lin, M. H. Lee, Z. P. Liu, C. T. Chen, C. J. Pickard, *Phys. Rev. B* **1999,** *60*, 13380-13389.
12. R. He, Z. S. Lin, M. H. Lee, C. T. Chen, *J. Appl. Phys.* **2011**, 109, 103510
13. Z. Lin, X. Jiang, L. Kang, P. Gong, S. Luo, M.-H. Lee, *J. Phys. D: Appl. Phys.* **2014,** *47*, 253001.
14. S. R. Bowman, S. O' Connor, N. J. Condon, *Opt. Express*, **2012**, 20, 12906-12911.
15. T. Jiang, Y. Chen, Y. Lin, X. Gong, J. Huang, Z. Luo, Y. Huang, *J. Lumin.*, **2018**, 199, 133-137.
16. F. Cornacchia, A. D. Lieto, M. Tonelli, A. Richter, E. Heumann, G. Huber, *Opt. Express*, **2008**, 16, 15932-15941.
17. M. Fibrich, H. Jelínková, J. Šulc, K. Nejezchleb, V. Škoda, *Appl. Phys. B*, **2009**, 97, 363-367.
18. J. Bartschke, K. -J. Boller, R. Wallenstein, I. V. Klimov, V. B. Tsvetkov, I. A. Shcherbakov, *J. Opt. Soc. Am. B*, **1997**, 14, 3452-3456.
19. Q. Ye, L. Shah, J. Eichenholz, D. Hammons, R. Peale, M. Richardson, A. Chin, B. H. T. Chai, *Opt. Commun.*, **1999**, 164, 33-37.
20. F. Mougel, G. Aka, A. Kahn-Harari, H. Hubert, J. M. Benitez, D. Vivien, *Opt. Mater.*, **1997**, 8, 161-173.
21. M. J. Lederer, M. Hildebrandt, V. Z. Kolev, B. Luther-Davies, B. Taylor, J. Dawes, P. Dekker, J. Piper, H. H. Tan, C. Jagadish, *Opt. Lett.*, **2002**, 27, 436-438.
22. H. Zhang, X. Meng, L. Zhu, P. Wang, X. Liu, R. Cheng, J. Dawes, P. Dekker, S. Zhang, L. Sun, *J. Cryst. Growth*, **1999**, 200, 335-338.
23. H. Jiang, J. Wang, H. Zhang, X. Hu, B. Teng, C. Zhang, P. Wang, *Chem. Phys. Lett.*, **2002**, 357, 15-19.
24. T. Schweizer, T. Jensen, E. Heumann, G. Huber, *Opt. Commun.*, **1995**, 118, 557-561.
25. N. A. Tolstik, V. E. Kisel, N. V. Kuleshov, V. V. Maltsev, N. I. Leonyuk, *Appl. Phys. B*, **2009**, 97, 357-362.
26. S. A. Payne, L. L. Chase, L. K. Smith, W. L. Kway, W. F. Kruple, *IEEE J. Quantum Elect.*, **1992**, 28, 2619-2630.
27. V. Petrov, J. Liu, M. Galan, G. Viera, C. Pujol, U. Griebner, M. Aguilo, F. Diaz, Proc. SPIE 6216, Laser Source and System Technology for Defense and Security II, 62160K (12 May **2006**)
28. W. Q. Shi, M. Bass, M. Brinbaum, *J. Opt. Soc. Am. B*, **1990**, 7, 1456-1462.
29. Y. Wang, Z. You, J. Li, Z. Zhu, E. Ma, C. Tu, *J. Phys. D: Appl. Phys.*, **2009**, 42, 215406.